

Localization of impulsive sources in the ocean using the method of images

Too Yuen Min and Mandar Chitre

Acoustic Research Laboratory, Tropical Marine Science Institute

National University of Singapore, 12A Kent Ridge Road, Singapore 119223

E-mail: {ymtoo, mandar}@arl.nus.edu.sg

Abstract—Impulsive transient signals produced by snapping shrimp dominate the high frequency ambient noise in warm shallow waters. A receiver not only observes the direct arrival of the snap from the shrimp, but also multipath reflections from scattering boundaries such as the sea surface, seabed, etc. We formulate a geometric model corresponding to one direct arrival and one surface reflection. The originating location of a snap can be extracted from the model if the exact position of each element in the receiver array is known. In practice, we only have coarse prior knowledge of the array depth and orientation, and the exact array element locations have to be estimated. The situation is further complicated by the fact that many snaps occur concurrently, and associating a snap with its reflection is a non-trivial problem. We use least logarithmic absolute (LLA) criteria to explore the unknown parameter in this joint estimation and association problem. The association can be further refined based on the complete geometric model. We outline our method and present a numerical simulation to test the performance of the estimator. Results from a dataset collected in Singapore waters using a broadband small-aperture phased array are illustrated. We compare the results with previous findings, demonstrating that accurate passive localization of known structures in the ocean using natural noise made by snapping shrimp inhabiting the structures can be achieved.

I. INTRODUCTION

Snapping shrimp produce impulsive noises with peak-to-peak source levels up to 190 dB ref 1 μ Pa @ 1 m, dominating a broad frequency spectrum of ambient noise ranging from 2 kHz to above 200 kHz [1] [2]. Localizing the sources of these signals has several potential applications in underwater acoustic sensing. For example, the clustering of snapping shrimp may provide information on location and health of coral reefs [3]. This is analogous to the detection of bustle in cities providing an indication of human activity. In ambient noise imaging (ANI), snapping shrimp are potential sources of opportunity to illuminate silent underwater objects. Given the estimated location of the source shrimp, it is possible to do passive ranging and multistatic sonar processing [4].

Localizing snapping shrimp remains a challenging problem especially using small aperture arrays. While the direction of sources can be determined when the sources are far away, determining the range to the source requires that the source be in the near-field of the array. Since the near-field is only a small multiple of the aperture of the array, large aperture arrays are required to obtain the range and bearing of snapping shrimp. While this approach has been used to locate shrimp over small ranges [5], Chitre et al. [4] estimated shrimp locations using

small aperture array with the assumption such that snapping shrimp live on a flat seabed. This assumption may not be valid in some scenarios and the exact knowledge of the local bathymetry is not always available. In this paper, our objective is to investigate a different approach to localization of shrimp in the far-field of a sensor array. We form an effectively larger virtual array consisting of the actual array and its image in the water surface by incorporating both the direct arrivals and surface reflections of snaps. This enables us to accurately localize sources in the far-field of the sensor array without the knowledge of the local bathymetry or the assumption that shrimp live on the seabed.

II. GEOMETRIC MODEL

A snap generates multipath propagations in warm shallow waters. The primary propagating path is the direct arrival. The first order propagating paths are the reflections at air-water interface and water-seabed interface, namely the surface and bottom reflections. The reflection coefficient is approximately -1 for a snap being reflected at the water-air interface so the surface reflection is, in the ideal case, the same as the direct arrival with 180° phase inversion [6]. Due to the high absorption loss, especially in areas with sandy seabed, the bottom reflection and higher order propagations are ignored. Hence, we formulate a geometric model corresponding to one direct arrival and its surface reflection. Water surface is assumed to be relatively calm and flat, and no assumption is made regarding the structure of the seabed. For the sake of brevity, direct arrival and the corresponding surface reflection are denoted as direct-reflection pair.

Figure 1 shows a 3-dimensional geometric model and the cross section in azimuth angle, ϕ , of direct-reflection of a snap. In this figure, the direct-reflection propagates in the same azimuth angle but this constraint will be relaxed when the direct-reflection association problem is introduced. In Figure 1(b), elevation angles of the direct-reflection are denoted by θ_d and θ_r respectively. Elevation angle, θ , carries a positive sign if it is above the orientation vector indicated by OA, a line perpendicular to the receiver. θ_o is the angle between the orientation vector and the OB line parallel to water surface. It carries a positive sign for angles above OB. r_d and r_r are the distances travelled from the origin of the snap to the receiver. The time of arrivals of the direct-reflection are τ_d and τ_r . Since the surface reflection has similar characteristics

as direct arrival, the snap detection process, which extracts snap direct arrival, $(\phi_d, \theta_d, \tau_d)$, from time-series sensors data, can be applied to find surface reflection, $(\phi_r, \theta_r, \tau_r)$ [4] [7]. We introduce a 6-tuple $(\phi_d, \theta_d, \tau_d, \phi_r, \theta_r, \tau_d)$ representation of direct-reflection of a snap.

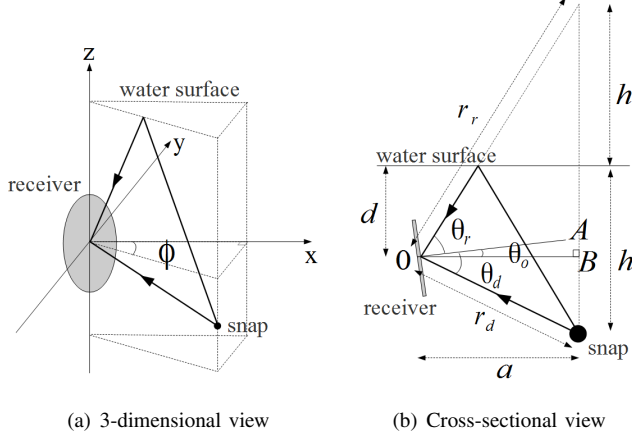


Fig. 1. Geometric model with two arrows indicating direct arrival and surface reflection of a snap. (a) shows a 3-dimensional direct-reflection of a snap. (b) shows the cross-sectional view at azimuth angle ϕ .

With the receiver steered at orientation angle, θ_o , we have

$$\cos(\theta_d + \theta_o) = \frac{a}{r_d}, \quad (1)$$

$$\cos(\theta_r + \theta_o) = \frac{a}{r_r} \quad (2)$$

and

$$\delta\tau = \frac{r_r - r_d}{c} \quad (3)$$

where $\delta\tau = \tau_r - \tau_d$ and c is the underwater speed of sound. (1)-(3) can be written compactly as

$$\delta\tau = \frac{a}{c} \left[\frac{1}{\cos(\theta_r + \theta_o)} - \frac{1}{\cos(\theta_d + \theta_o)} \right]. \quad (4)$$

Equating the two vertical distances, h , we derive

$$|d - a \tan(\theta_d + \theta_o)| = a \tan(\theta_r + \theta_o) - d. \quad (5)$$

By squaring both sides of (5) and selecting the non-trivial solution, we obtain

$$a = \frac{2d}{\tan(\theta_d + \theta_o) + \tan(\theta_r + \theta_o)}. \quad (6)$$

Substituting (6) into (4) yields

$$\delta\tau = \frac{2d}{c} \left[\frac{\cos(\theta_d + \theta_o) - \cos(\theta_r + \theta_o)}{\sin(\theta_d + \theta_r + 2\theta_o)} \right] \quad (7)$$

which is the direct-reflection time delay. r_d can be estimated as

$$r_d = \frac{2d \cos(\theta_r + \theta_o)}{\sin(\theta_d + \theta_r + 2\theta_o)} \quad (8)$$

based on (1) and (5) provided receiver depth, d , and orientation, θ_o , are known. The location vector of the snap is

$$\Lambda = \begin{bmatrix} \frac{2d \cos(\phi_d)}{\tan(\theta_d + \theta_o) + \tan(\theta_r + \theta_o)} \\ \frac{2d \sin(\phi_d)}{\tan(\theta_d + \theta_o) + \tan(\theta_r + \theta_o)} \\ \frac{2d \tan(\theta_d + \theta_o)}{\tan(\theta_d + \theta_o) + \tan(\theta_r + \theta_o)} \end{bmatrix} \quad (9)$$

according to the Cartesian coordinate system in Figure 1. θ_o is based on the structure of the seabed where the receiver is located at. For a static receiver, it is a constant and is measurable using either an active sonar or an accelerometer. Hence, we assume that θ_o is known a priori. Due to the rise and fall of the tides at different times, d can vary within a few meters in a day. The prior knowledge of average depth, d_{ave} , maximum depth, d_U , and minimum depth, d_L , are known but not the exact depth, d .

III. SNAP LOCALIZATION

To determine the snapping shrimp locations, there are two pieces of crucial information that need to be estimated in practice. One is the unknown receiver depth, d of the geometric model. The other is the association of direct-reflection snaps from multiple arrivals. In this section, we outline a method to solve this joint estimation and association problem. At first, coarse pairing rules are introduced based on physical properties of surface reflection to eliminate many of the incorrect pairings. For the rest of the possible pairings, we formulate an optimization problem where the error between measured and modeled time delays is minimized to estimate receiver depth of the geometric model. Then, the coarse pairs are refined by greedy selection.

A. Coarse pairing

If $2N$ arrivals are observed, we can form, at most, $4N^2 - 2N$ coarse pairs but they comprise a large portion of wrong pairs as $N \gg 1$. When the number of arrivals increases, the number of wrong pairs become predominant among the coarse pairs. Three pairing rules are used to filter out the obvious wrong pairs. They are essentially based on the physical properties of surface reflection such as

- 1) $\phi_d - \epsilon_\phi \leq \phi_r \leq \phi_d + \epsilon_\phi$,
- 2) $\theta_r > |\theta_d|$,
- 3) $0 \leq \delta\tau \leq \frac{2d_U}{c}$.

The azimuth angle of reflection, ϕ_r , has to be within a small deviation, ϵ_ϕ , from the direct, ϕ_d . The elevation angle of reflection, θ_r , has to be greater than the magnitude of the elevation angle of the direct arrival, $|\theta_d|$. Direct-reflection time delay, $\delta\tau$, is a positive real value, bounded by property 3. The upper bound is achieved when the snap is located on the seabed below the receiver at $a = 0$ from Figure 1. Given $2N$ arrivals denoted as $(\phi_j, \theta_j, \tau_j)$ where $j = 1, \dots, 2N$, we select K coarse pairs which satisfy the aforementioned properties denoted as $(\phi_{k,d}, \theta_{k,d}, \tau_{k,d}, \phi_{k,r}, \theta_{k,r}, \tau_{k,d})$ where $k = 1, \dots, K$ and $K \leq N$.

B. Receiver depth estimation

The 6-tuple representation of coarse pairs contains estimation error introduced by arrival detection process and extreme noise of wrong pairs. Hence, we only have the estimated 6-tuple representation, $(\hat{\phi}_{k,d}, \hat{\theta}_{k,d}, \hat{\tau}_{k,d}, \hat{\phi}_{k,r}, \hat{\theta}_{k,r}, \hat{\tau}_{k,d})$ for $k = 1, \dots, K$. Optimal estimator is almost intractable for the nonlinear model in (7). Standard least squares estimator is vulnerable to the wrong pairs error. We know that d must be within a lower bound, d_L , and upper bound, d_U , due to the limit of tidal change. The distribution of direct-reflection time delay of coarse pairs is asymmetric and positively skewed. This argument can be shown in Figure 5. An estimator minimizing the sum error of the bulk of data is formulated as

$$\hat{d} = \arg \min_{d_L \leq d \leq d_U} \sum_{k=1}^K \log \left(\left| \delta \hat{\tau}_k - \frac{2d}{c} \left[\frac{\cos(\hat{\theta}_{k,d} + \theta_o) - \cos(\hat{\theta}_{k,r} + \theta_o)}{\sin(\hat{\theta}_{k,d} + \hat{\theta}_{k,r} + 2\theta_o)} \right] \right| \right). \quad (10)$$

This is a bounded-variable least logarithmic absolute (LLA) estimator. In fact, it is a special case of myriad estimator with mode-like behaviour as the tuning constant, p , is zero [8]. The LLA criteria imposes milder cost on the data points that deviate from the bulk of data. The performance of LLA is discussed in the numerical simulation.

C. Refinement

The coarse pairs are refined by selecting the direct-reflection pair which has smallest time delay square error defined as

$$e_k = \left(\delta \tau_k - \frac{2\hat{d}}{c} \left[\frac{\cos(\hat{\theta}_{k,d} + \theta_o) - \cos(\hat{\theta}_{k,r} + \theta_o)}{\sin(\hat{\theta}_{k,d} + \hat{\theta}_{k,r} + 2\theta_o)} \right] \right)^2 \quad (11)$$

for $k = 1, \dots, K$. Then, all the coarse pairs, which contain any of the chosen direct-reflection arrivals, will not be considered in the subsequent selection. This greedy selection repeats until there is no time delay square error greater than the threshold, ϵ_e . A possible data dependent threshold is the boundary between data cluster, E_a , and noise cluster, E_b . Let $E = \{e_1, \dots, e_K\}$, $E_a \subset E$ with centroid c_a and $E_b \subset E$ with centroid c_b . Since $E_a \cap E_b = \{\emptyset\}$, the threshold can be computed as

$$\epsilon_e = \min_{\tilde{e} \in E_a} [|\tilde{e} - c_b|]. \quad (12)$$

IV. RESULTS AND DISCUSSIONS

A. Numerical simulation

The performance of snap localization is verified in the following simulation. 300 snaps were uniformly generated based on:

- $\phi_d \sim \mathcal{U}[-60^\circ, +60^\circ]$
- $a \sim \mathcal{U}[20 \text{ m}, 200 \text{ m}]$
- $z \sim \mathcal{U}[0 \text{ m}, -20 \text{ m}]$

where a is the horizontal distance from the receiver and z is the depth of the source from the sea level. 300 surface reflections

were obtained referring to the geometric model. Zero-mean independent and identically distributed (IID) Gaussian noises with standard deviation, σ_v , were added to the azimuth and elevation angle of the simulated arrivals. For simplicity, the noise for times of arrival was omitted. All the direct and reflection arrivals were detected as $(\phi_k, \theta_k, \tau_k)$ for $k = 1, 2, \dots, 600$. The coarse pairing was applied and d was estimated using LLA and least absolute (LA) estimator for comparison. The coarse pairs were refined and snap locations were computed based on the estimated d using LLA and LA. In this simulation, θ_o was known and the simulated results were collected by averaging out 100 realizations with $d = 13 \text{ m}$.

Figure 2 shows the percentages of average number of wrong pairs. There are approximately 36% of wrong pairs at zero noise and it reaches 73% for $\sigma_v = 5$. The number of wrong pairs is significant even though there is no noise added. This indicates that the proposed coarse pairing rules might be too general such that some of the wrong pairs were still counted in for zero noise scenario. The mean absolute error, $\text{MAE} = \frac{1}{100} \sum_{j=1}^{100} [|d - \hat{d}_j|]$, of LLA and LA estimators is shown in Figure 3. LLA outperforms LA in estimating d over all the noise standard deviations. Both estimators have similar performance for small noise standard deviation ($0^\circ \leq \sigma_v \leq 1.5^\circ$). The MAE of LA starts to increase abruptly when $\sigma_v > 1.5^\circ$. At $\sigma_v = 5$, the MAE of LA grows to 7 m while that of LLA remains around 1.2 m. Given the estimated snap locations, $\hat{\Lambda}_l$, where $l = 1, \dots, L$, error of snap location, ξ , is defined as

$$\xi = \frac{1}{L} \sum_{l=1}^L \|\Lambda_l^* - \hat{\Lambda}_l\|_2 \quad (13)$$

where Λ_l^* is the actual snap location corresponding to $\hat{\Lambda}_l$ and $\|\cdot\|_2$ is the Euclidean distance. In Figure 4, the performances of snap localization based on LA and LLA are similar for small σ_v . For $\sigma_v > 1.5^\circ$, ξ increases tremendously under LA compared to LLA.

B. Experimental results

In contrast to conventional source localization method developed in [5], snap localization can be performed using small aperture array by associating the direct and reflection arrivals. [4] relies on the assumption that snapping shrimp are located on a flat seabed. Our proposed geometric model does not assume a flat seabed nor that snapping shrimp should stay on the seabed. We compare our method with [4] based on a 30-second ROMANIS¹ dataset collected on April 11, 2010 at 21:04:55 local time in the seabed with average depth of 15 m.

To detect the arrivals [4], 0.5 fractile of the sensor signal envelop is chosen to compensate for the weak surface reflection. We identify 2129 arrivals. With $\epsilon_\phi = 2^\circ$ and $d_U = 20 \text{ m}$, we apply the pairing algorithm and 481 coarse direct-reflection pairs are obtained. The direct-reflection time delay is shown in Figure 5. These data points consist of several correct direct-

¹2D planar array with 1.3 m diameter [4].

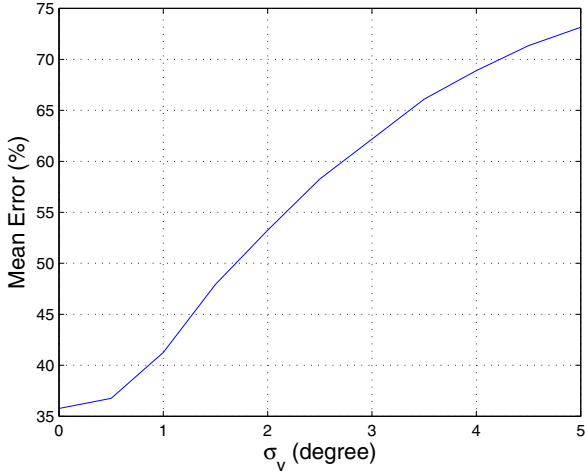


Fig. 2. Mean percentage of wrong pairs in coarse pairing corresponds to noise standard deviation.

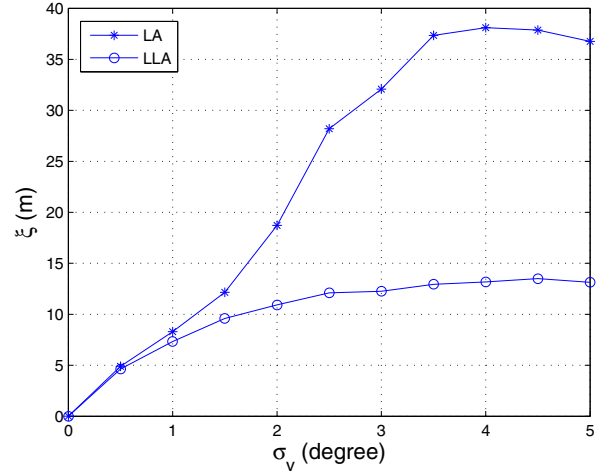


Fig. 4. Error of the snap localization based on \hat{d} using LA and LLA.

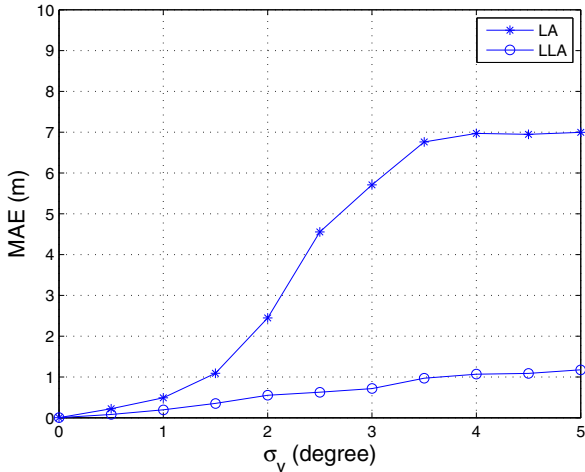


Fig. 3. MAE of \hat{d} using LA and LLA with noise standard deviation from 0° to 5° .

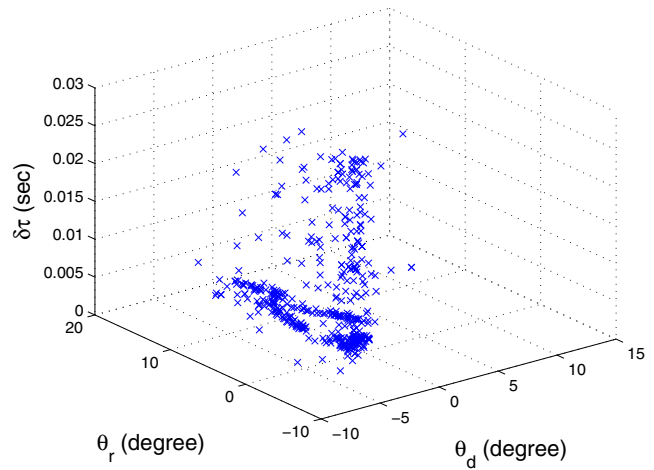


Fig. 5. Scatter plot of the geometric model based on the coarse direct-reflection pairs.

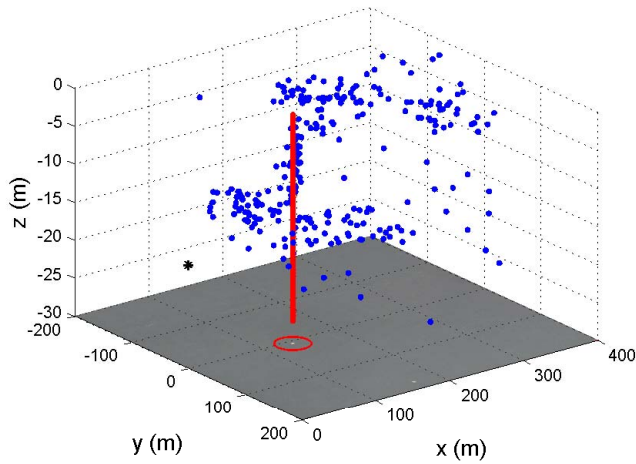
reflection pairings, and some outliers which are perhaps wrong pairings. The plane-like cluster represents the geometric model while the data points above the cluster are probably the wrong pairs. A geometric model with \hat{d} is selected to fit the cluster. Let $\theta_o = 2.29^\circ$, $d_L = 10$ m, $d_U = 20$ m, \hat{d} is 16.4826 m using LLA. The coarse pairs are refined and 277 locations of snaps are estimated as shown in Figure 6. The Cartesian coordinate system of the geometric model is modified such that the origin of z-axis is set to be on the water surface while x- and y-axes remain the same for better illustration. Given ROMANIS was positioned at $1^\circ 12.967'N, 103^\circ 44.382'E$, we crop and superimpose the respective area from map on Figure 6. The map shows a long-term mooring buoy (tiny white dot at this scale, highlighted by us with an ellipse). We have plotted a vertical line above the map at the location of the buoy. Snapping shrimp seem to be present in clusters and one of

these clusters originated from the snapping shrimp lodged on the long-term mooring buoy.

We compare the result with previous finding [4] in Figure 7. By assuming that the seabed is flat and snapping shrimp are colonizing the seabed, [4] shows that a large number of snaps arrive from an azimuth angle of 2.4° , however the estimated range of the snaps seem to be inaccurate. Our method manages to unveil the long-term mooring buoy at the range of approximately 135 m from ROMANIS. This matches the location of the mooring buoy in the superimposed map. Note that nearby snaps are undetectable. There is no snap within the 80 m range as shown in the Figure 7(a). One of the possible reasons is the sensitivity of the directional sensors in the ROMANIS array at large angles. The surface reflection of a nearby snap has large elevation angle. This weakens the arrivals and causes most of them to be missed by the arrival detection algorithm.



(a) Long-term mooring buoy

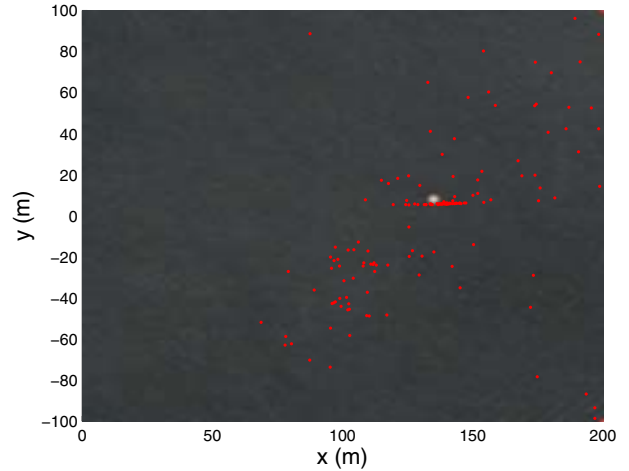


(b) Estimated snap locations

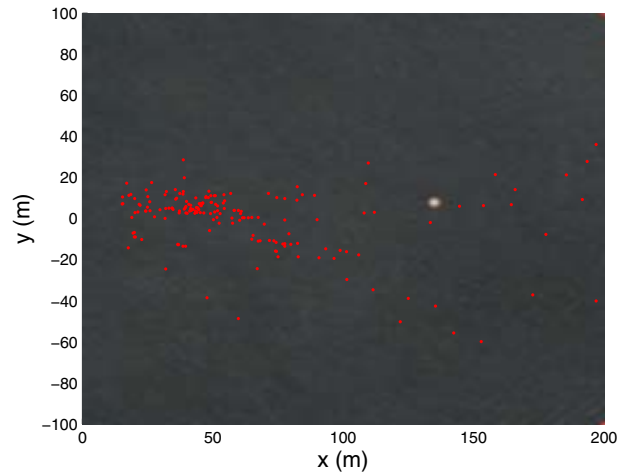
Fig. 6. (a) is a photograph showing a mooring buoy, visible in front of the ROMANIS. In (b), the dots show the estimated spatial distribution of the shrimp and the vertical line illustrates the x-y position of the long-term mooring buoy. The location of ROMANIS is represented by an asterisk.

V. CONCLUSION

We have formulated a geometric model based on method of images and outlined a snapping shrimp localization method. Numerical simulation result shows that the estimation of receiver depth based on coarse pairs is reliable. The pairings can be refined using the resulting model, and the location of the shrimp can be determined from the pairs. Applying the method to a dataset from an experiment with a 1.3 m array allowed us to visualize a man-made structure inhabited by shrimp at a range of about 135 m from our array. Although the proposed method possesses advantage over the wavefront curvature method, it comes with the degradation of localization accuracy. Constructing the uncertainty of the snap location with respect to the error of time of arrivals is not straight forward. However, the proposed method is capable of revealing the rough locations of snapping shrimp clusters using small aperture array and we are looking for potential applications of



(a) Method of images



(b) Method from [4]

Fig. 7. Comparison of estimated shrimp locations between (a) the proposed method and (b) method in [4] within a $200\text{ m} \times 200\text{ m}$ area in front of the ROMANIS. The white dot in the map is the long-term mooring buoy.

the ambient sources with their estimated locations.

ACKNOWLEDGMENT

We would like to thank Mr. Subash, Ms. Tan Soo Pieng, Mr. Naveen, Mr. Mohan, Mr. Unnikrishnan, Dr. Venugopalan and numerous other colleagues at ARL for their support in the development of ROMANIS and during the field experiments. We would also like to thank Ms. Ong Lee Lin for proofreading the paper.

REFERENCES

- [1] W. W. Au and K. Banks, "The acoustics of the snapping shrimp *synalpheus parneomeris* in kaneohe bay," *The Journal of the Acoustical Society of America*, vol. 103, no. 1, pp. 41–47, 1998.
- [2] J. R. Potter, T. W. Lim, and M. Chitre, "High-frequency ambient noise in warm shallow waters," *Sea Surface Sound, UK*, 1997.
- [3] M. Chitre, M. Legg, and T.-B. Koay, "Snapping shrimp dominated natural soundscape in singapore waters," 2012.

- [4] M. Chitre, S. Kuselan, and V. Pallayil, "Ambient noise imaging in warm shallow waters; robust statistical algorithms and range estimation," *The Journal of the Acoustical Society of America*, vol. 132, no. 2, pp. 838–847, 2012.
- [5] B. G. Ferguson and J. L. Cleary, "In situ source level and source position estimates of biological transient signals produced by snapping shrimp in an underwater environment," *The Journal of the Acoustical Society of America*, vol. 109, p. 3031, 2001.
- [6] L. M. Brekhovskikh and Y. Lysanov, *Fundamentals of ocean acoustics (3rd edition)*. Springer-Verlag, 2003.
- [7] K. T. Beng, T. E. Teck, M. Chitre, and J. R. Potter, "Estimating the spatial and temporal distribution of snapping shrimp using a portable, broadband 3-dimensional acoustic array," in *OCEANS 2003. Proceedings*, vol. 5. IEEE, 2003, pp. 2706–2713.
- [8] G. R. Arce, *Nonlinear signal processing: a statistical approach*. John Wiley & Sons, 2005.